Materials Advances

ROYAL SOCIETY OF CHEMISTRY

PAPER

View Article Online
View Journal | View Issue

Cite this: *Mater. Adv.*, 2024, 5, 5781

Cu-containing polyoxometalate-based melamine in the environmental remediation of toxic organic pollutants†

Nahal Aramesh and Bahram Yadollahi *

Harmful industrial pollutants are the most important and substantial challenges in ecological and environmental processes. Therefore, environmental remediation of these types of toxic materials is an important issue. The main purpose of the present study is the catalytic reduction of some organic dyes and nitro aromatic compounds as toxic contaminants in the presence of polyoxometalates (POMs). At first, the transition metal-substituted Keggin-type POM-based melamine was prepared and identified using different techniques such as FTIR, XRD, TGA, and FE-SEM. Then, the catalytic performance of these synthesized compounds in the reduction of some nitro aromatic compounds and organic dyes was investigated. By copper-substituted Keggin-type POM-based melamine (CuPOM@melamine), the best result was obtained with higher conversion and shorter reaction time. All reactions were carried out using $NaBH_4$ as the reducing reagent at room temperature and in water as solvent. Furthermore, the apparent rate constants were determined by considering pseudo first-order kinetic studies for these reactions. The main purpose of the present study is introducing an impressive way to eliminate hazardous industrial pollutants using POM-based melamine. The choice of melamine as a support for increasing the surface area, electron transfer ability and catalytic activity is another important aspect of this purpose. This effective system was used in water as the solvent and at room temperature. Easy preparation, nontoxicity, simple to operate, low-cost, environmentally friendly, and efficient catalytic activities are priorities of this system that could be applied in the environmental processes.

Received 21st February 2024,
Accepted 30th May 2024

DOI: 10.1039/d4ma00178h

rsc.li/materials-advances

1. Introduction

With the fast development of industries and appearance of serious environmental challenges in particular accumulation of toxic organic pollutants with difficult degradability, the design of appropriate catalytic systems for the removal of toxicant contaminants from industrial activities has increased. The progress of these systems is essential for the development of valuable catalysts with suitable properties such as availability, low cost, non-toxicity, and eco-friendliness. This feature not only could decrease hazardous pollutants from natural environment but also increase safety measures to improve the quality of living conditions.[1] Among different pollutants, nitro aromatic compounds and aromatic dyes encompass the remarkable classes and main sources of contaminants due to their high carcinogenic and toxic nature, non-biodegradability and commercial matters. Therefore, the removal of these types of pollutants plays a valuable role in the field of ecological and environmental systems. Until now, for the removal of these toxic organic compounds, various methods have been employed, such as coagulation–flocculation,[2] extraction,[3] photocatalytic degradation,[4] adsorption,[5] and chemical redox.[6] However, these methods have some problems such as time-consuming processes, slowness, low performance, high cost, and by-product construction. Among these procedures, catalytic reduction in the presence of appropriate catalysts is a promising approach to destroy the toxic contaminants and convert them into non-toxic compounds because of its simplicity, ease of operation, availability, and economy. For instance, Liu *et al.* designed a magnetically separable and highly-dispersed PdNi nanoparticle-modified N-doped mesoporous carbon nanocatalyst for the degradation of 4-nitrophenol (4-NP).[7] In another study, Gao *et al.* investigated the catalytic performance of three-dimensional silver/polyethyleneimine/alginate hydrogel beads for the hydrogenation reaction of 4-NP under batch and fixed-bed experiments.[8] These composites were synthesized by a one-pot electrostatic assembly method. Moreover, a novel core–shell-structured Ag-based magnetic functional polymer nanocatalyst, Fe_3O_4@SN/GLA@chitosan–Ag (SN =

Department of Chemistry, University of Isfahan, Isfahan 81746-73441, Iran.
E-mail: yadollahi@chem.ui.ac.ir, yadollahi.b@gmail.com

† Electronic supplementary information (ESI) available. See DOI: https://doi.org/10.1039/d4ma00178h

amino-functionalized SiO_2, and GLA = glutaraldehyde), was fabricated by utilizing the stabilization function and reducing ability of renewable chitosan macromolecules *in situ*.[9] This system exhibited superior catalytic performance and long-term stability in the reduction of 4-NP. The reduction of organic dyes in the presence of the magnetic Fe_3O_4/Cu nanocomposite was also evaluated.[10] This hybrid nanocatalyst showed excellent catalytic activity and high stability in recycled reactions.

Polyoxometalates (POMs) are well-known and interesting species of inorganic metal–oxygen clusters that have gained much attention due to their high negative charge, numerous surface oxygen atoms, plentiful active sites, low cost, nontoxic nature, redox potentials, and high stability.[11] In terms of diverse utilizations, their catalytic performance is the most common and prevalent application. Hence, they are considered as promising and eco-friendly catalysts in many fields involving cycloaddition reactions,[12] ring-opening reactions,[13] olefin hydrocarboxylation reaction,[14] degradation,[15] water splitting,[16] oxidation reactions,[17] reduction reactions,[18] and others. Despite the unique POM properties, their catalytic activities have some limitations, such as low surface area and high solubility in aqueous solutions. One of the simple and feasible approaches to overcome these problems and to create efficient POM-based materials is the use of various solid supports, including metal nanoparticles,[19] metal oxides,[20] porous framework materials,[21] carbon materials and so on. These POM-based materials could increase their catalytic performance, providing suitable chemical sites, surface area, and electron transfer ability.

Amongst different supports, melamine (a triazine aromatic ring) as a cheap, crystalline, thermally stable, and nitrogen-rich (more than 65%) substance could be used as an intriguing candidate to modify the catalytic performance. Due to the existence of multiple amino functional groups and their strong binding ability, melamine could form various composites with different materials without any additional assistance. Recently, the application of melamine-based materials as efficient catalysts has been investigated in the removal of toxic compounds and dyes. For instance, the elimination of phenolic compounds with substantial activities and high adsorption capacities was performed in the presence of melamine/polyaniline-derived carbons (MPDCs).[22] Akbari *et al.* prepared a melamine-based porous network thin film containing Pd, and reported its applicability and effective catalytic performance in the nitro phenols (NPs) reduction and dyes degradation.[23] Moreover, the polyvinyl alcohol/melamine-formaldehyde composite was fabricated by Bhat *et al.* as a good adsorbent for the adsorption of Congo red (CR) dye.[24] In another study, Wang *et al.* demonstrated the high catalytic activity of palladium stabilized on melamine-functionalized magnetic chitosan composites in the reduction of *p*-NP with good reusability and degradability.[25]

Currently, catalytic reduction of toxic compounds using POM catalysts has also achieved much attention. For example, Jiao *et al.* reported on a new Zn-containing $[SiZnW_{11}O_{39}]^{6-}$ Keggin polyanion in 2,4,6-tri(4-pyridyl)-1,3,5-triazine (TPT) framework with high photocatalytic performance in the selective reduction of nitrobenzene.[26] In another work, Kurbah investigated the excellent catalytic activities and good selectivity of a POM/nickel oxide nanocomposite in the reduction of nitroarenes.[27] Furthermore, a POM redox mediator was applied for the reduction of nitro benzenes to anilines with high selective electrocatalytic activity at room temperature in aqueous solution without any sacrificial reagents.[28] In another study, a heterogeneous magnetic nanocatalyst, $[Fe_3O_4@SiO_2–NH_2–Cu_{20}P_8W_{48}]$, with excellent yield in the reduction of NPs into the corresponding aminophenols was demonstrated.[29] We were interested in studying the catalytic performance of transition metal-substituted POMs (MPOMs) with unique properties in these kinds of reactions. In order to make a proper system based on MPOMs and resolve some of their problems, melamine was chosen as a solid support. For this purpose, in the present work, transition metal-substituted Keggin-type POMs/melamine-based networks (MPOMs@melamine; M = Cr, Fe, Mn, Ni, Co, Zn, and Cu) were synthesized, and their catalytic performances in the reduction reactions of toxic dyes and nitro aromatic compounds were considered. The aim of the present work is to eliminate some poisonous compounds and change them into nontoxic compounds using POMs/melamine-based materials.

2. Experimental

2.1. Materials and characterizations

All materials, such as chemicals, reagents, and solvents (including metal salts, melamine (2,4,6-triamino-1,3,5-triazine), sodium borohydride ($NaBH_4$), nitro aromatic compounds, and organic dyes), were commercially accessible and purchased from authentic chemical companies. They were used with no additional purification steps. Various techniques were applied for the characterization of the synthesized compounds. Fourier transform infrared (FTIR) spectra were obtained with a JASCO 6300 FTIR spectrometer (400–4000 cm^{-1}). A thermogravimetric analyzer TG50 was used for thermogravimetric analysis/differential thermal analysis (TGA/DTA) under air atmosphere with a heating rate of 10 °C min^{-1} (25–800 °C). The X-ray diffraction (XRD) patterns were obtained on a Bruker diffractometer instrument (D8 advance) with Ni-filtered Cu Kα radiation (λ = 1.54178 Å). The UV-vis spectra of the nitro aromatic compounds and organic dyes during the reduction reactions were recorded by a Varian 5A spectrophotometer. The elemental mapping and field-emission scanning electron microscopic (FE-SEM) analyses were obtained by a Mira3 TESCAN. Inductively coupled plasma optical emission spectroscopy (ICP-OES) was performed on a PerkinElmer Optima 7300 DV ICP-OES spectrometer.

2.2. Preparation of MPOMs@melamine compounds

At first, an aqueous solution of $[PW_{11}MO_{39}]^{n-}$ was prepared. For this purpose, to a solution of $Na_2WO_4{\cdot}2H_2O$ (100 mmol) and Na_2HPO_4 (9.1 mmol) in 200 mL deionized water was added 12 mmol metal nitrate (MNO_3, in which M is Cr, Fe, Mn, Ni, Co, Zn, or Cu) under stirring. The pH of the solution was adjusted to 4.8 in order to prepare the $[PW_{11}MO_{39}]^{n-}$ aqueous solution.[30] After that, melamine (15 g) was added slowly to the above solution and to complete the reaction stirring for 12 h.

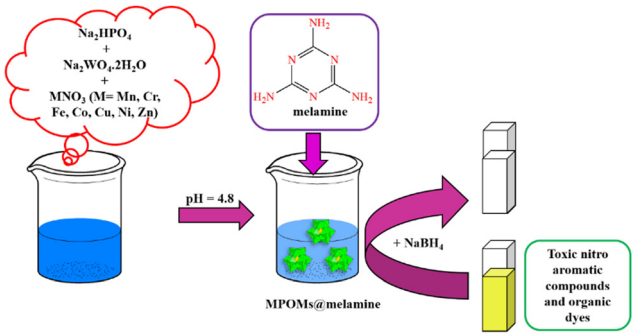

Fig. 1 Schematic illustration of the MPOMs@melamine (where M is Cr, Fe, Mn, Ni, Co, Zn, or Cu) synthesis procedure and its application as a catalyst.

Finally, the obtained solids as MPOMs@melamine (in which M is Cr, Fe, Mn, Ni, Co, Zn, or Cu) compounds were filtered and washed 2–3 times using deionized water, and dried in air.

2.3. Catalytic reduction of toxic nitro aromatic compounds and organic dyes by MPOMs@melamine

A 3 mL quartz cuvette was charged by an aqueous solution of organic dye or nitro aromatic compound (2 mL, 0.1 mM) and aqueous solution of $NaBH_4$ (100 μL, 15 mM) at room temperature. After that, the MPOMs@melamine (where M is Cr, Fe, Mn, Ni, Co, Zn, or Cu) catalyst in solution (40 μL, 1 mM) was added and the reduction reaction was initiated. The reaction progress was monitored by UV-vis spectrophotometer. The solution color was gradually changed from yellow to colorless by the progress of reaction. Furthermore, simultaneous catalytic reduction of some dye mixtures was performed in the same procedure. A schematic representation of the MPOMs@melamine (where M is Cr, Fe, Mn, Ni, Co, Zn, or Cu) synthesis route and its utilization as catalyst are shown in Fig. 1.

3. Results and discussion

In the present study, the MPOMs@melamine (where M is Cr, Fe, Mn, Ni, Co, Zn, or Cu) were prepared by a simple, green, and effective approach at room temperature, and they were applied as efficient catalysts in the reduction reaction of some toxic organic dyes and nitro aromatic compounds. The most important reason for the choice of MPOMs is their special properties, such as the numerous surface oxygen atoms, plentiful active sites, low cost, high electron transfer ability, redox potentials, non-toxicity nature, ease of operation, and environmental friendliness. These properties make them interesting in various catalytic systems. The use of POMs in the catalytic reduction reaction of toxic compounds has not been extensively reported. This could be owing to some limitations, including high solubility in aqueous solution and low surface area. In order to overcome these problems and improve the catalytic activity of POMs, melamine as a solid support was chosen. Melamine is a cheap and thermally stable compound with the existence of multiple amino functional groups in its structure and strong binding ability.

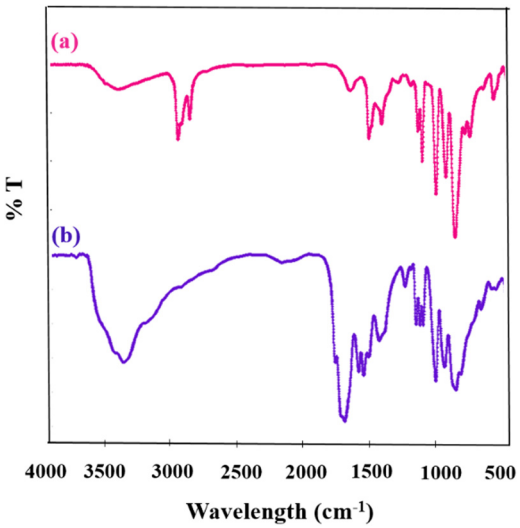

Fig. 2 The FT-IR spectra of CuPOM (a) before and (b) after the addition of melamine (CuPOM@melamine).

3.1. Synthesis and characterization of MPOMs@melamine catalysts

Initially, the chemical structures of the as-synthesized compounds were identified by FTIR spectra. Fig. 2 shows the FTIR spectra of $[PW_{11}CuO_{39}]^{5-}$ (CuPOM) and $[PW_{11}CuO_{39}]^{5-}$@melamine (CuPOM@melamine). The absorption bands appearing in the scope of 500–1100 cm^{-1} are assigned to the characteristic fingerprints of POMs that confirm the stretching regions of P–O, Cu–O, W–O, and W–O–W.[31]

The absorption bands of melamine are positioned in three regions. First, the broad bands at 3000–3500 cm^{-1} belong to the N–H stretching modes derived from the free and hydrogen bonded amino groups.[32] Second, several bands in the 1100–1700 cm^{-1} region are attributed to the stretching modes of C–N, C═N, and 1,3,5-*s*-triazine aromatic rings. The bending mode of NH_2 is located at 1650 cm^{-1}. Third, a band at 808 cm^{-1} is ascribed to the out of plane bending mode of 1,3,5-*s*-triazine ring.[33] Furthermore, the bands appeared from 400–750 cm^{-1} are attributed to C–NH_2, in which the weakening of these peaks could confirm the occurrence of pre-polymerization.[23,34] Also, as indicated, the presence of melamine and the maintained structure of POM in the prepared CuPOM@melamine catalyst are revealed.

The XRD patterns of CuPOM, melamine, and CuPOM@melamine are exhibited in Fig. S1 (ESI†). It is clear that the Keggin-type POM structures can be defected into lacunary species by the loss of one or several metal–oxygen groups from the metal oxide cluster. The XRD patterns of the lacunary ones are totally different from the XRD patterns of the Keggin-type POM structures, as reported by Shringarpure *et al.*[35] Moreover, additional peaks and some changes are found for MPOMs due to the incorporation of transition metals into the lacunary position of POMs.[36] As can be seen in Fig. S1a (ESI†), the characteristic diffraction bands of CuPOM at 2θ = 7–8°, 19–25°, and 30° are shown.[37] In the XRD pattern of melamine (Fig. S1b, ESI†), the

peaks appearing at about 13°, 15°, 18°, 22°, 23°, 27°, and 29° corresponded to the (100), (011), (110), (11−2), (012), (021), and (21−2) crystalline planes, respectively. According to the XRD pattern of CuPOM@melamine in Fig. S1c (ESI†), the diffraction peaks of POM and melamine are preserved, which could confirm the conservation of the POM structure after the formation of CuPOM@melamine. Moreover, a comparison was made between the XRD patterns for melamine and CuPOM@melamine (Fig. S1b and c, ESI†). Obvious changes in the intensity and the full width at half maximum of the peaks related to the (100), (011), (110), and (021) crystalline planes and the disappearance of the (11−2), (012), and (21−2) crystalline planes in the XRD pattern of CuPOM@melamine can be observed, which provides support for the polymerization process.[23,34] Therefore, both the XRD patterns and FTIR spectrum displayed direct proof for the pre-polymerization event that occurred at room temperature.

To evaluate the thermal stability of CuPOM@melamine, TG-DTG analysis was used as a valuable method. The investigation on the thermal behavior of CuPOM@melamine was done under air atmosphere with 10 °C min^{-1} heating rate from 25 to 800 °C. As shown in Fig. 3, the weight loss happened in three separate stages. In the first stage, the weight loss from 45 to 220 °C is due to the elimination of solvent (such as water) from the structure. Similar to the previous studies,[23,38] the second loss weigh from 225 to 400 °C and the third loss weight in the temperature range of 415–600 °C are ascribed to the thermal decomposition of melamine. The multiple oxidative decomposition processes of the intermediate products were completed before 600 °C.

Table S1 (ESI†) shows the elemental analysis, and Fig. S3 and S4 (ESI†) exhibit the elemental mapping and FE-SEM images of CuPOM@melamine in order to investigate its composition and structure. The images confirm the presence of Cu, P, O, W, N, and C elements, which are attributed to the CuPOM and melamine. Thus, the successful synthesis of CuPOM@melamine is approved.

There are different possible interactions between melamine and POM. (1) Because of the existence of multiple amino functional groups in the structure of melamine, it can be readily polymerized. The extensive intermolecular hydrogen bonds in melamine cause it to form a network structure[23] in which POM can get stuck and trapped. (2) On the other hand, electrostatic and hydrogen bonding interactions may occur between the anionic metal–oxo group of POM clusters and melamine that can operate in a synergistic manner and presumably form superstructures.[39] (3) Moreover, melamine can display strong binding ability by multiple binding sites consisting of the three aromatic ring nitrogen atoms and three exocyclic amino groups.[40,41] Three primary amine groups with electron-rich nitrogen atoms can act as chelating ligands and are most likely bound onto the electron-deficient surface of the transition metal through the coordinating interactions.[42] In addition, three nitrogen atoms of the aromatic ring in the melamine structure can show strong binding affinity to transition metals,[43] and serve as the pyridine-like compounds and a molecular linker.

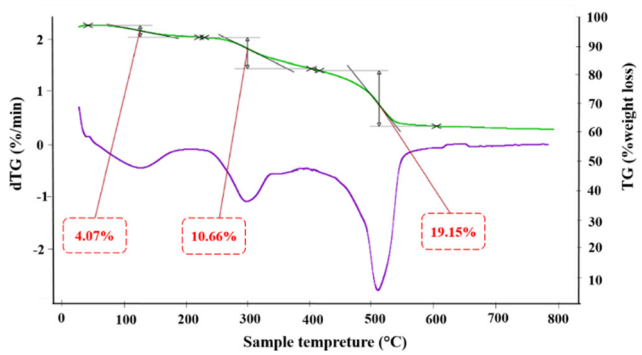

Fig. 3 The CuPOM@melamine TG/DTG curve.

3.2. The catalytic reduction studies

3.2.1. Catalytic reduction of 4-NP and optimization of the reaction conditions. After the synthesis and characterization of MPOMs@melamine (where M is Cr, Fe, Mn, Ni, Co, Zn, and Cu), their catalytic performances in the reduction reaction of nitro aromatic compounds and organic dyes were evaluated. Nitro aromatic compounds are carcinogenic, toxic, persistence, and harmful materials. They are extensively applied in the laboratories and industrial processes, and have also caused considerable effects on environmental and ecological systems. Furthermore, organic dyes (especially azo dyes) are another group of toxic materials for environment and living organisms because of the substituted aromatic rings in their structures.[44] Therefore, the catalytic reduction of organic dyes and nitro aromatic compounds is a valuable issue, and has achieved significant importance. The major purpose of these type of reactions is to modify toxic materials into nontoxic ones in order to remove the environmental pollutants and improve the living quality conditions. On the other hand, the obtained amino aromatic compounds could be used as considerable materials in the preparation of several polymers, drugs, pharmaceutical compounds, *etc.*[45] The MPOMs@melamine (where M is Cr, Fe, Mn, Ni, Co, Zn, and Cu) were chosen as suitable catalysts for these reduction reactions owing to their unique properties, such as low-cost, easy synthesis and operating, nontoxicity nature, environmentally friendship, good redox potentials, effective electron donor–acceptor, and high electron transfer abilities.

At first, different reaction parameters were checked in order to get the best results and optimized experimental conditions. For this purpose, the catalytic activities of MPOMs@melamine (where M is Cr, Fe, Mn, Ni, Co, Zn, and Cu) were examined in the catalytic reduction of 4-NP as a typical example of these reactions. UV-vis spectroscopy was used to follow the progress of the reaction with time. The catalytic reduction reactions of 4-NP were performed using $NaBH_4$ as the reducing agent and MPOMs@melamine (where M is Cr, Fe, Mn, Ni, Co, Zn, and Cu) as the catalyst at room temperature in water. For the aqueous solution of 4-NP, a maximum absorption band appeared at

317 nm. Adding $NaBH_4$ to the 4-NP solution caused a change in the position of the absorption band from 317 nm to 400 nm, which is called a red shift (Fig. S5, ESI†).[46] This red shift could be attributed to the creation of the negatively charged oxygen owing to the formation of 4-nitrophenolate ions. This negative charge could delocalize in the structure more than the unshared pair of electrons.[47] It was found that the use of a catalyst is indispensable, and these types of reduction reactions are not started in the absence of catalyst. When only the reducing agent was present, there was no remarkable change in the intensity of absorption peak with time.

By adding the MPOMs@melamine (where M is Cr, Fe, Mn, Ni, Co, Zn, and Cu) catalyst to the reaction solution, the reduction reaction was initiated. The intensity of the maximum absorbance band without any change in the position was gradually decreased with the progress of the reaction. Moreover, as the absorbance peak of 4-nitrophenolate at 400 nm decreased, a new absorbance peak located at 295 nm appeared at the same time (Fig. 4(a)). Thus, it can be considered that MPOMs@melamine (where M is Cr, Fe, Mn, Ni, Co, Zn, and Cu) catalysed the reduction reaction of 4-NP into 4-AP. The reduction progress was monitored by absorption *versus* wavelength curves during the reaction. It is worth mentioning that the bright yellow color of the solution at the end of the reaction was changed to colorless. Both the main reactants and products are UV-visible-active species. Thus, the conversion of the nitro-group into the corresponding amino group can be confirmed by the complete disappearance of the nitro group absorption peak from the reactants with the cocomitant appearance of a new absorption peak at the characteristic wavelength of the amino group. The product analysis was also completed with nuclear magnetic resonance spectroscopy after the reduction reaction.

To achieve the optimum reaction conditions in the catalytic reduction of 4-NP, the efficacy of several factors on the catalytic activity of MPOMs@melamine was examined. In the first step, the catalytic effect of different transition metal-substituted Keggin-type POMs in MPOMs@melamine (where M is Cr, Fe, Mn, Ni, Co, Zn, and Cu) on this catalytic reaction system was investigated. According to the obtained information (Table 1, entries 1–7), the copper-substituted POM catalyst, CuPOM@melamine, is the most active catalyst with a higher conversion and shorter reaction time. In comparison, other MPOMs@malamine were given lower catalytic performances. In addition, a negligible catalytic conversion was seen for the reduction of 4-NP using just melamine and MPOMs under the same reaction conditions.

Table 1 The results of 4-NP reduction under different conditions after 12 min

Entry	Catalyst	Catalyst extent (μL)	$NaBH_4$ (μL)	Conversion (%)
1	CrPOM@melamine	40	100	5
2	MnPOM@melamine	40	100	5
3	FePOM@melamine	40	100	10
4	CoPOM@melamine	40	100	5
5	NiPOM@melamine	40	100	20
6	**CuPOM@melamine**	**40**	**100**	**95**
7	ZnPOM@melamine	40	100	5
8	CuPOM@melamine	20	100	30
9	CuPOM@melamine	30	100	65
10	CuPOM@melamine	50	100	90
11	CuPOM@melamine	40	80	20
12	CuPOM@melamine	40	90	35
13	CuPOM@melamine	40	110	90

In the second step, the catalytic reductions of 4-NP were evaluated by different amounts of CuPOM@melamine catalyst (50, 40, 30, and 20 μL, 1 mM solution). As can be seen in Table 1 (entries 6 and 8–10), the reaction conversions, as anticipated, are enhanced by increasing the catalyst content. The catalytic reaction in this system was almost completed with 40 μL of catalyst. Thus, this catalyst amount was selected as the optimum value. Additionally, no considerable change in the reaction conversion was exhibited with higher amounts of catalyst.

In the next step, the influence of the reducing agent amount on the reaction conversion was tested in the presence of different amounts of $NaBH_4$ (80, 90, 100, and 110 μL of 15 mM solution). The results in Table 1 (entries 6 and 11–13) indicate that the catalytic activity of CuPOM@melamine increased by increasing the $NaBH_4$ amount. The best conversion in this catalytic system was shown by 100 μL of $NaBH_4$. As the amount of $NaBH_4$ increased, the content of the reduction product remained almost fixed. Thus, a higher amount of $NaBH_4$ did not have a remarkable effect on the catalytic performance.

The UV-vis spectra for the catalytic reduction of 4-NP under optimized conditions by CuPOM@melamine as a catalyst at 2 min intervals are shown in Fig. 4(a). During the progress of the reaction, there is a clear decline in the absorption peak intensity at 400 nm and appearance of a new peak at 295 nm. To calculate the reduction percentage of the nitro aromatic compounds in this catalytic system, the following equation was used:

$$\text{Reduction percentage} = 100 - [A_t \times 100/A_0]$$

In this equation, A_t is the absorption amount at time t, and A_0 is the absorption at the beginning of reaction. These calculations were performed based on the original absorbance peak of the nitro aromatic compounds. Fig. 4(b) represents

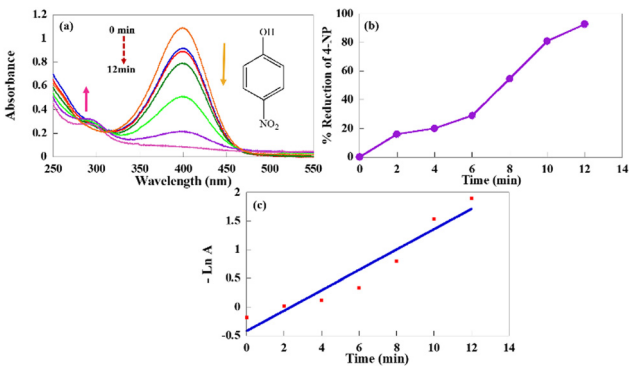

Fig. 4 (a) The UV-vis spectra for the reduction of 4-NP with $NaBH_4$ at every 2 min in the presence of CuPOM@melamine as the catalyst at room temperature, (b) the reduction percent of 4-NP, and (c) $-\ln A$ *versus* time plot for the kinetic examination.

different reduction percentages of 4-NP *versus* time. As can be seen, the reduction percents are increased with time. It demonstrates that the CuPOM@melamine catalyst could accomplish 95% reduction of 4-NP with $NaBH_4$ after 12 min. Also, the kinetic study of the nitro aromatic compound reductions was assessed in order to evaluate the rate constant of the reduction reactions. For this purpose, pseudo-first-order kinetics was used to investigate the reduction reaction rate owing to the lower concentration of the nitro aromatic compounds with respect to the $NaBH_4$ concentration. The concentration of $NaBH_4$ was considered to be in excess and constant in order to not have an effect on the rate of the reactions. The plot of $-\ln A$ (absorption at maximum wavelength) *versus* time for the 4-NP catalytic reduction is shown in Fig. 4(c). The linear relationship between these two parameters confirms the pseudo-first-order kinetics for this system. The determined rate constant from the slope is 1.77×10^{-1} min^{-1}.

3.2.2. Catalytic reduction of other nitro aromatics. Afterwards, the catalytic performances of CuPOM@melamine in the reaction of other NP derivatives (Fig. S6, ESI†) containing 3-nitrophenol (3-NP), 2-nitrophenol (2-NP), 4-nitroaniline (4-NA), 2-nitroaniline (2-NA), and 2,4-dinitrophenol (DNP) were examined in order to expand the catalyst application. The UV-vis spectra with and without $NaBH_4$ for aqueous solutions of other nitro aromatic derivatives are demonstrated in Fig. S7 (ESI†).

For instance, two characteristic peaks of the 2-NP aqueous solution are at 275 and 350 nm. The red shifts from 275 and 350 nm to 282 and 415 nm after the addition of $NaBH_4$ are a result of the formation of 2-nitrophenolate. Like 4-NP, the reducing agent alone was unable to reduce the solution of 2-NP, and the reaction did not start in the absence of the catalyst. In contrast, the gradual decline in the intensity of the 2-NP peak located at 415 nm was initiated after the addition of the catalyst.

As shown in Fig. 5(a), the absorption peak at 415 nm disappeared with time, indicating the catalytic reduction of 2-NP into the corresponding amine (2-aminophenol; 2-AP).[48] The reduction percentage of 2-NP with time was also considered (Fig. 5(b)). As can be seen, about 90% reduction of 2-NP was completed after 20 min reaction in the presence of $NaBH_4$. Moreover, the apparent rate constant for the 2-NP reduction was measured by pseudo-first-order kinetics study (7.33×10^{-2} min^{-1}), as shown in Fig. 5(c).

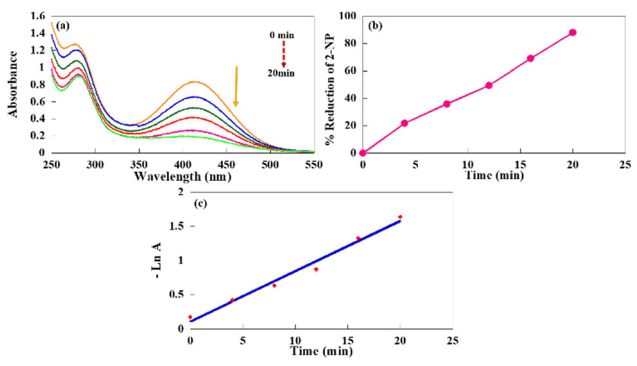

Fig. 5 (a) The UV-vis spectra for the reaction of 2-NP at every 4 min in the presence of CuPOM@melamine under optimized conditions. (b) The reduction percent of 2-NP, and (c) $-\ln A$ *versus* time plot for the kinetic examination.

As stated above, the catalytic performance of CuPOM@melamine in the reduction of other NP derivatives (including DNP, 3-NP, 4-NA, and 2-NA) was also checked. Obviously, the same catalytic effects happened. The reduction systems did not perform without the presence of the catalyst despite extended reaction times. According to Fig. 6, similar observations with 4-NP were also recorded. As can be seen, the decline of the NPs maximum absorption peaks is shown after the addition of the catalyst. The reactions are followed by UV-vis spectrophotometry at certain intervals of time. In all reactions, the characteristic peaks of NPs disappeared with time, and NPs were converted to the analogue aminophenols. The reduction percentages and apparent reaction rate constants of different NP derivatives are summarized in Table 2.

Pursuant to the obtained results in Table 2, all NP derivatives showed a successful reduction of the nitro moiety into the corresponding amino groups with very good to excellent conversions (85–95%) within 10–30 min. Moreover, it was found that the place of the nitro group on the aromatic ring as *ortho*, *meta*, and *para* has an effect on the reactivity of NPs. So, from the results in Table 2 (entries 1–3), the obtained reduction percentages and reaction rates for the catalytic reduction of 2-NP and 4-NP using CuPOM@melamine are higher than 3-NP. This could be ascribed to the resonance stability and electron delocalization in the aromatic ring of the 2-NP and 4-NP structures. In contrast, the nitro group electrons in 3-NP could not contribute in the conjugation. Furthermore, the reduction of 4-NP compared with 2-NP was performed in a shorter reaction time with higher reduction percentage and reaction rate. This is because there is less steric obstruction of the NO_2 group and more resonance stability of the structure. As a result, the reduction reaction rate trend for NPs in the presence of CuPOM@melamine are as follows: 4-NP > 2-NP > 3-NP.

The catalytic reduction of 4-NA and 2-NA, as other NP derivatives, in this system was also investigated. The resulting data in Table 2 (entries 4 and 5) indicate a faster reduction reaction with a shorter reaction time for 4-NA with respect to 2-NA. As mentioned above, it is assumed that the steric effect has an effective role on the reaction rate. Therefore, the reduction of 2-NA was slower than 4-NA due to the existence of steric hindrance in its structure and more difficult electron transfer. Additionally, the DNP compound was reduced into the corresponding diamine with excellent yield after 28 min (Table 2, entry 6). Consequently, it is evident that CuPOM@melamine exhibited efficient catalytic performance in the reduction reaction of various nitro aromatic compounds.

3.2.3. Catalytic reduction reaction of organic dyes. Organic dyes have been used in different activities, such as painting, printing, plastics, and cosmetics. They are well-known pollutants for the environment and ecosystem, and their release into the environment is an important challenge for the living organisms and human health. Also, they are

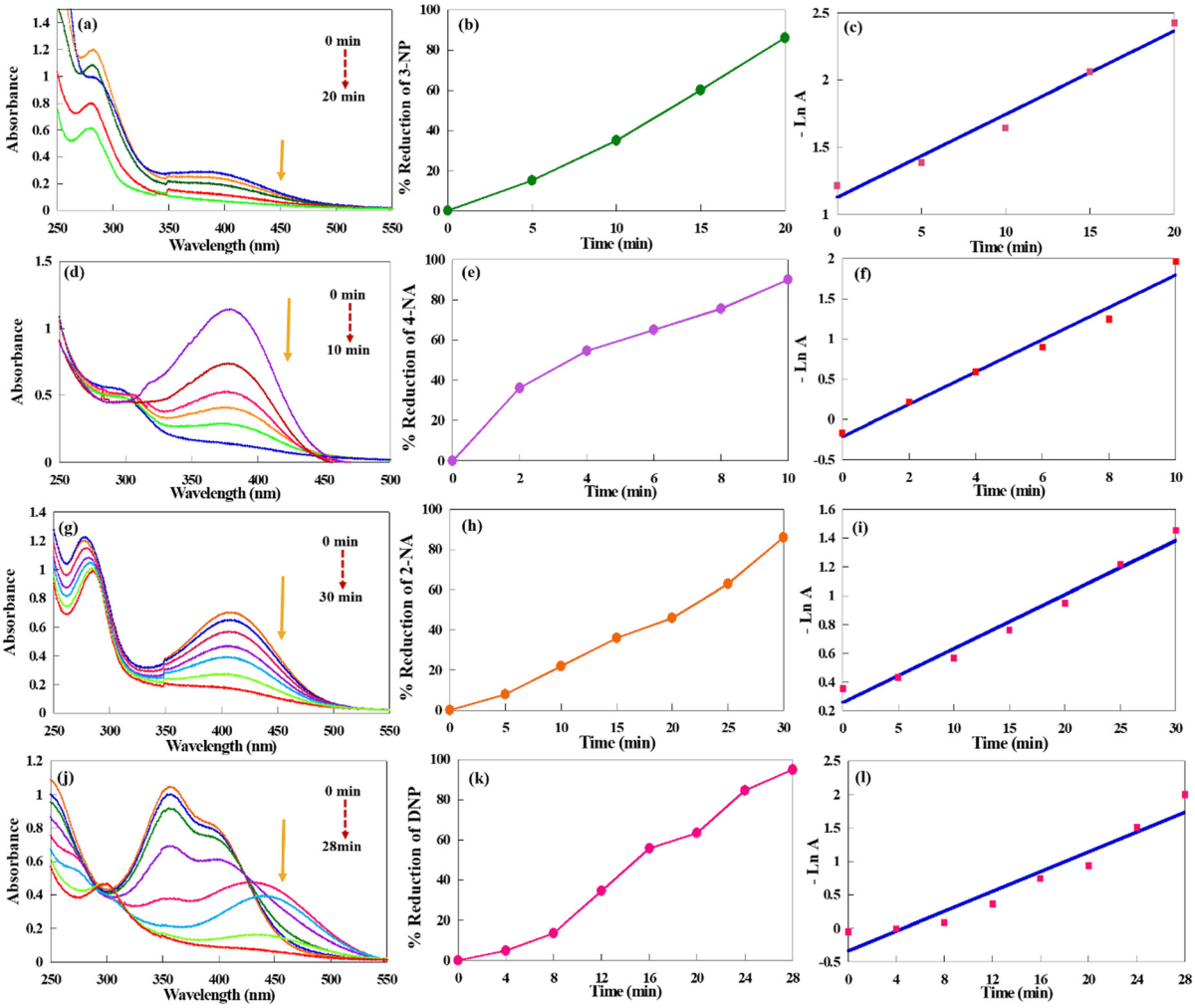

Fig. 6 The UV-vis spectra for the catalytic reduction of (a) 3-NP at every 5 min, (d) 4-NA at every 2 min, (g) 2-NA at every 5 min, and (j) DNP at every 4 min; the reduction percent of (b) 3-NP, (e) 4-NA, (h) 2-NA, and (k) DNP; and $-\ln A$ *versus* time plots for (c) 3-NP, (f) 4-NA, (i) 2-NA, and (l) DNP reductions for the kinetic study.

Table 2 The reaction times, apparent rate constants, and reaction percentages for the catalytic reduction of various nitro aromatic compounds (0.1 mM) with $NaBH_4$ (15 mM) and the CuPOM@melamine catalyst

Entry	Nitro aromatic compound	Reaction time (min)	Reduction percent (%)	Apparent rate constant (min^{-1})
1	4-NP	12	95	1.77×10^{-1}
2	3-NP	20	85	6.21×10^{-2}
3	2-NP	20	90	7.33×10^{-2}
4	2-NA	30	85	3.76×10^{-2}
5	4-NA	10	90	2.00×10^{-1}
6	DNP	28	95	7.38×10^{-2}

non-biodegradable compounds owing to the presence of substituted aromatic rings in their structures. Therefore, the reduction reactions of organic dyes are considered as a valuable process in environmental remediation. In this study, the catalytic reductions of methyl orange (MO), methylene blue (MB), congo red (CR), and rhodamine B (RhB) with CuPOM@melamine were investigated. MO is an anionic azo dye and common indicator in the laboratory with low biodegradability, high toxicity and carcinogenic nature.[49] The aqueous solution of MO shows a strong absorption band centered at 466 nm and a weak absorption peak at 275 nm. With the addition of $NaBH_4$, the intensity of the absorption peaks remains unchanged even after hours have passed.[50] However, a decline in intensity of both absorption peaks was observed after the addition of the CuPOM@melamine catalyst when the catalytic reaction was followed by UV-vis spectroscopy (Fig. 7).

From the results in Fig. 7(a), the MO absorption peaks gradually decreased. Concomitantly, a new peak at 246 nm appeared with the progress of the process. At the end of the reaction, two absorption peaks of MO vanished due to the azo bond (–N═N–) cleavage. A new absorption peak at 246 nm appeared, which was related to the produced amino compounds (Fig. 7(d)).[51] In addition, the color of the solution was altered from orange to colorless. These observations confirmed that CuPOM@melamine could act as an effectual catalyst for the catalytic reduction of MO. As indicated in Fig. 7(b), the

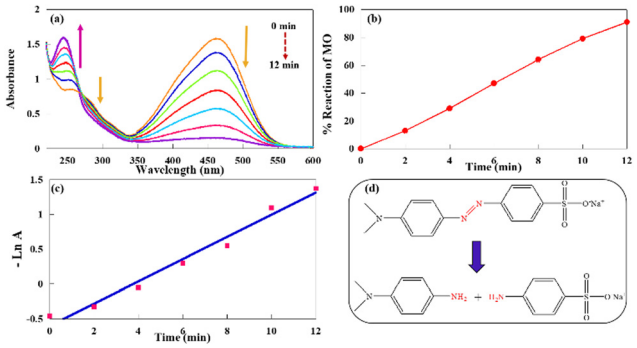

Fig. 7 (a) The UV-vis spectra of the MO catalytic reduction with $NaBH_4$ using CuPOM@melamine at every 2 min. (b) The reduction percent of MO, (c) The plot of $-\ln A$ *versus* time for the kinetic examination, and (d) The possible reduction reaction of MO.

reaction of MO was about 90% completed after 12 min. Additionally, the pseudo-first-order kinetics was used to measure the reaction rate, as it was similar to the nitro aromatic compounds. As mentioned above, the slope of the absorbance at the maximum wavelength (λ = 466 nm) as a function of time (Fig. 7(c)) was calculated to achieve the apparent rate constant (1.82×10^{-1} min^{-1}).

Likewise, the catalytic performance of CuPOM@melamine in the reactions of CR, MB, and RhB was evaluated. The UV-vis spectra for the catalytic reductions of CR, MB, and RhB aqueous solutions are demonstrated in Fig. 8. As with MO, no notable change in the intensity of the absorption peaks is seen in the absence of catalyst. From Fig. 8, it can be seen that the intensity of the maximum absorption peaks of the dyes is decreased after the addition of the catalyst and disappeared with time. All reactions were done at room temperature and in water as solvent. Their apparent reaction rate constants and reaction percentages are summarized in Table 3. Moreover, the possible suggested reaction routes for the catalytic reduction of MB, RB, and CR dyes according to the literatures are displayed in Fig. S8 (ESI†).[49,52,53]

According to Table 3, the reaction of various organic dyes using CuPOM@melamine was performed in appropriate reaction times (6–12 min) with high-to-excellent reaction percentages (91–98%) at room temperature. As shown in Table 3, the reaction rates of MB and RhB are higher than the MO and CR dyes. This can be ascribed to the charge of the dyes. The MB and RhB dyes are cationic, while MO and CR are considered as anionic azo dyes. Due to the existence of anionic POM clusters and electron-rich areas in the melamine network, cationic dyes could reduce more easily than anionic ones. Additionally, MO demonstrated a higher reaction rate than CR (Table 3, entries 1 and 2). It is clear that MO and CR dyes have one and two azo groups in their chemical structures, respectively. Hence, owing to the existence of more azo groups in the structure of CR and the greater complexity of the CR structure with respect to MO, its reaction being more difficult and slower. In general, it could be concluded from the obtained results that CuPOM@melamine demonstrated effective catalytic performance in the reduction reactions of both organic dyes and nitro aromatic

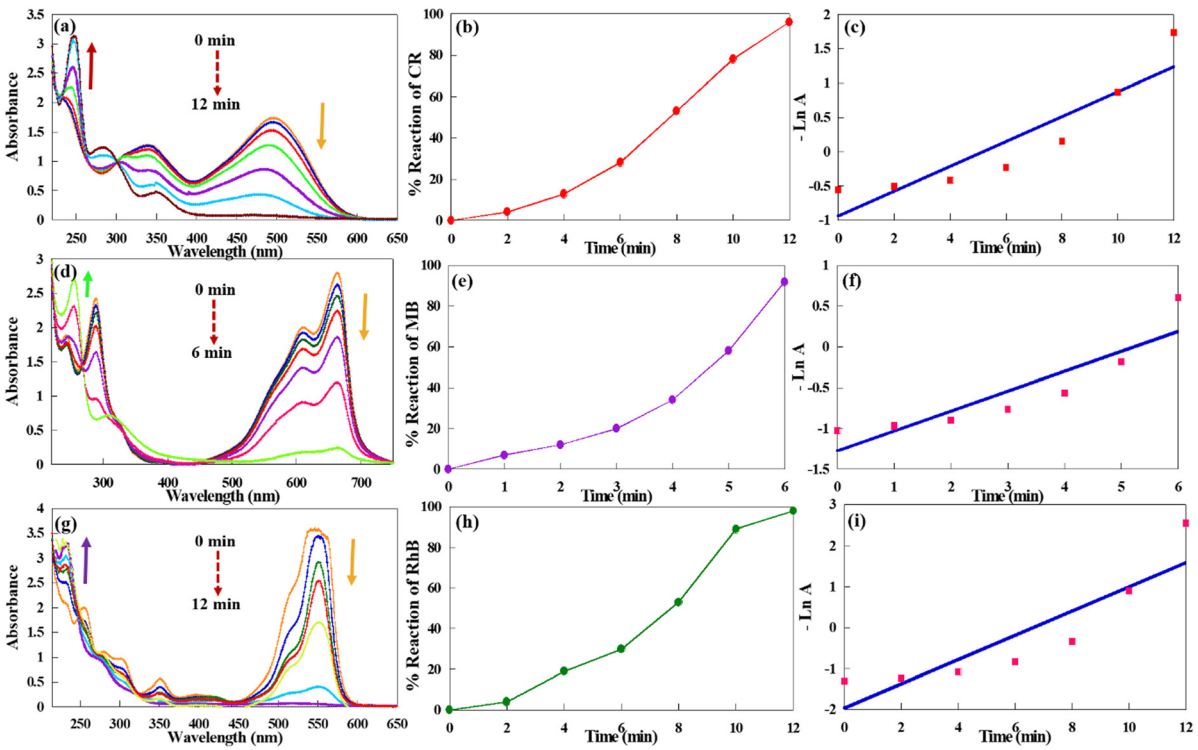

Fig. 8 The UV-vis spectra for the catalytic reactions of (a) CR at every 2 min, (d) MB at every 1 min, and (g) RhB at every 2 min; the reactions percent of (b) CR, (e) MB, and (h) RhB; and $-\ln A$ *versus* time plots of (c) CR, (f) MB, and (i) RhB reactions for the kinetic examination.

Table 3 The reaction percentages and rate constants for the reduction of some organic dyes (0.1 mM) using $NaBH_4$ (15 mM) and CuPOM@melamine as catalyst

Entry	Organic dye	Reaction time (min)	Reduction percent (%)	Apparent rate constant (min^{-1})
1	MO	12	90	1.82×10^{-1}
2	CR	12	95	1.60×10^{-1}
3	MB	6	92	2.96×10^{-1}
4	RhB	12	98	2.43×10^{-1}

compounds with short reaction times and high reaction percentages.

A plausible mechanism for the catalytic reduction of nitro aromatic compounds and organic dyes using the CuPOM@melamine catalyst with $NaBH_4$ as a hydrogen source is illustrated in Fig. 9. As indicated in Fig. 9, after the adsorption of BH_4^- and reactants on the surface of the catalyst, the reduction take place through the transfer of electrons from the hydride ions into the reactants with the help of the catalyst. In fact, the main role of the catalyst is to improve the electron transfer ability. Since POMs have good electron acceptability and excellent redox properties and melamine is an electron-rich compound, the CuPOM@melamine catalyst can facilitate the electron transfer to the reactants.

A comparative study between CuPOM@melamine and some of the recently reported catalysts is given in Table 4. For instance, the apparent rate constants for the catalytic reduction of 4-NP in the presence of CuPOM@g-C_3N_4 (8.64×10^{-2} min^{-1})[18] and Ru/H_xMoO_{3-y} (6.30×10^{-2} min^{-1})[54] are lower than our system (Table 4, entries 1, 2, and 5). Furthermore, the catalytic performance of NiO@Poly-Mo[27] and Mn-POM@MIL-100 (Fe)[55] in the reduction of 4-NP was followed at 100 °C and 50 °C, respectively, while the catalytic reduction of 4-NP in our system was performed at room temperature (Table 4, entries 1, 3, and 6). Also, our system indicated a shorter reaction time and higher conversion in comparison with the NiO@PolyMo nanocatalyst for the reduction of 4-NP (Table 4, entries 1 and 3). As can be seen, the reported previous catalytic systems for the removal of MO and MB dyes are investigated under light irradiation conditions (Table 4). However, our system needed no irradiation for the catalytic removal of organic dyes. Moreover, in comparison with other prior reported systems, our system exhibited shorter reaction times for the catalytic removal of MO and MB dyes. Also, the apparent rate constants for the removal of MO in the presence of PAA-PVA/$H_3PW_{12}O_{40}$@UiO-66 (3.00×10^{-2} min^{-1})[56] and for the removal of MB in the presence of CuO–ZnO (1.70×10^{-2} min^{-1})[57] and TCPP/CuPOM/TiO_2 (1.16×10^{-2} min^{-1})[58] are lower than our system (Table 4, entries 7 and 9–12). Therefore, CuPOM@melamine could act as a beneficial catalytic system toward the removal of toxic organic pollutants.

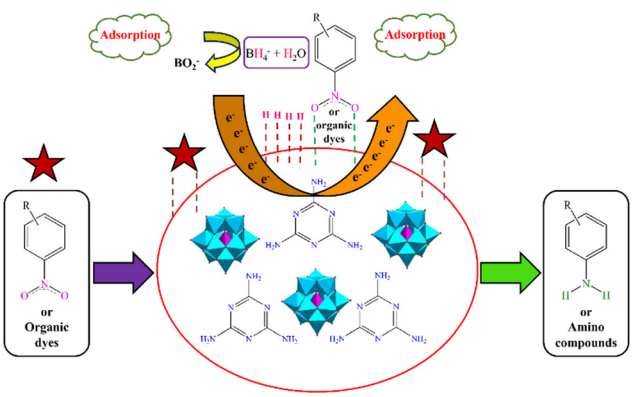

Fig. 9 The proposed mechanism for the catalytic reduction of nitro aromatic compounds and organic dyes using CuPOM@melamine catalyst.

Finally, the catalytic reduction of three mixtures of dyes was also investigated to evaluate the ability of CuPOM@melamine in the simultaneous reaction of two dyes. For this purpose, we examined the reactions of MO and MB, MO and MR, as well as CR and RhB, as three mixtures of selected dyes, in the presence of CuPOM@melamine and $NaBH_4$. In the aqueous solution of MO and MB, two maximum absorbance peaks respectively at 466 nm and 664 nm related to MO and MB dyes were seen. These absorbance peaks were stable in the presence of $NaBH_4$ alone. By addition of the CuPOM@melamine catalyst into the dye mixtures, the characteristic peaks of the dyes were gradually decreased with increasing time (Fig. 10). As shown in Fig. 10(a), the intensity of the MB characteristic peak at 664 nm first decreased. This peak vanished after 6 min and the catalytic reaction of MB was about 99% completed. After that, the decline in the intensity of the MO absorbance peak at 466 nm was initiated. This peak also disappeared and the reaction of MO was 90% accomplished 25 min after the start of the reaction. In addition, a new peak at 254 nm with a gradual increase in its intensity appeared during the reaction. This peak confirms the catalytic reduction of the MO and MB dye mixture in the presence of CuPOM@melamine.

Likewise, the catalytic activities of CuPOM@melamine in the reaction of MO and CR, along with CR and RhB mixtures, were studied. The mixture of MO and CR dyes gave only a strong absorption peak at 477 nm, instead of two characteristic absorption peaks of MO and CR at 466 nm and 496 nm (Fig. 10(b)). According to the previous report,[60] this observation is probably owing to the chemical interaction between these two dyes. Moreover, the solution of the CR and RhB mixture showed an absorption peak at 551 nm that was attributed to the RhB dye and two absorption peaks at 514 and 350 nm.

These two latter absorption peaks could be related to the CR dye, which are shifted to the longer wavelengths owing to the chemical interaction between the two dyes (Fig. 10(c)). In both reactions, the absorption peaks remained steady with only $NaBH_4$ and in the absence of catalyst. However, the intensity of the as-mentioned peaks decreased continuously with time in the presence of CuPOM@melamine, as shown in Fig. 10(b) and (c). At the same time, a new peak at 245 nm appeared, and its intensity increased with the reaction progress. According to the data, the reactions of the MO and CR dyes and of the CR and RhB dyes progressed to 95% and 93% completion after 30 min, respectively. Hence, from these results, CuPOM@melamine

Table 4 Comparison of different catalytic systems for the 4-NP reduction and removal of MO and MB dyes

Entry	Catalyst	Temperature (°C) or irradiation	Reactant	Conversion (%)	Reaction time (min)	Apparent rate constant (min^{-1})	Ref.
1	CuPOM@melamine	25	4-NP	95	12	1.77×10^{-1}	This work
2	CuPOM@g-C_3N_4	25	4-NP	90	25	8.64×10^{-2}	18
3	NiO@Poly-Mo	100	4-NP	60	240	NR[d]	27
4	Fe_3O_4@SiO_2–NH_2–$Cu_{20}P_8W_{48}$	25	4-NP	100	10	NR[d]	29
5	Ru/H_xMoO_{3-y}	25	4-NP	NR*	45	6.30×10^{-2}	54
6	Mn-POM@MIL-100 (Fe)	50	4-NP	96	12	2.30×10^{-1}	55
7	CuPOM@melamine	—	MO	90	12	1.82×10^{-1}	This work
8	3-API/MnPOM[a]	Visible light	MO	89.9	180	NR[d]	59
9	PAA-PVA/$H_3PW_{12}O_{40}$@UiO-66[b]	UV light	MO	97.35	120	3.00×10^{-2}	56
10	CuPOM@melamine	—	MB	92	6	2.96×10^{-1}	This work
11	CuO–ZnO	Visible light	MB	76	105	1.70×10^{-2}	57
12	TCPP/CuPOM/TiO_2[c]	Visible light	MB	49	100	1.16×10^{-2}	58

[a] 3-(Aminopropyl)-imidazole (3-API). [b] Polyacrylic acid (PAA)-poly(vinyl alcohol) (PVA). [c] Tetra(4-carboxyphenyl)porphyrin (TCPP). [d] NR = not reported.

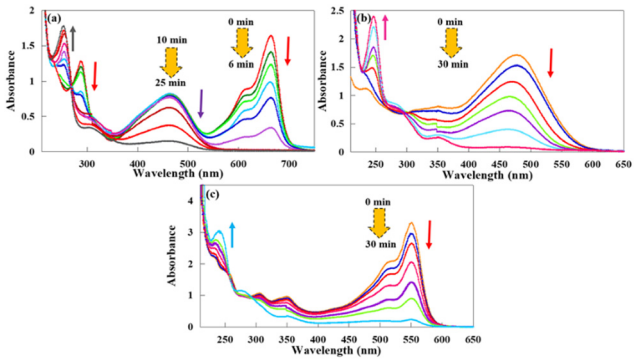

Fig. 10 The UV-vis spectra for the catalytic reactions of (a) MO and MB, (b) MO and CR, and (c) CR and RhB at room temperature.

could act as an appropriate and effective catalyst in the reduction reaction of dye mixtures at room temperature.

4. Conclusions

In this work, MPOM@melamine (where M is Cr, Fe, Mn, Ni, Co, Zn, and Cu) compounds were synthesized by a facile and simple procedure. After characterization, they were successfully used in the catalytic reduction of toxic organic pollutants as harmful, carcinogenic and challenging compounds for ecological and environmental systems. The CuPOM@melamine catalyst showed impressive catalytic activity in the reduction reaction of some nitro aromatic compounds containing 4-NP, 2-NP, 3-NP, 2-NA, 4-NA, and DNP, as well as different organic dyes (such as MO, CR, MB, and RhB), and also the mixtures of these dyes (like MO and MB, MO and CR, and also CR and RhB). All reactions were performed with $NaBH_4$ as a reducing agent in water as a green solvent and at room temperature. There are several advantages to this system, including its availability, low cost, simple operation, nontoxicity, environmental friendship, good redox potentials, high capability of electron transfer, and excellent reaction percentages (up to 98%) and times (6–30 min). Considering these properties, this process exhibits promising potential for the reduction of an extensive scope of toxic pollutants.

Author contributions

The study conception and design, material preparation, data collection and analysis were performed by Nahal Aramesh and Bahram Yadollahi. The first draft of the manuscript was written by Nahal Aramesh and Bahram Yadollahi, and they read and approved the final manuscript.

Conflicts of interest

There are no conflicts to declare.

Acknowledgements

The authors are thankful to the University of Isfahan and Iran National Science Foundation (INSF; grant no. 98015776) for their support.

References

1 A. Balakrishnan and M. Chinthala, Comprehensive review on advanced reusability of g-C_3N_4 based photocatalysts for the removal of organic pollutants, *Chemosphere*, 2022, **297**, 134190.
2 Y.-Y. Lau, Y.-S. Wong, T.-T. Teng, N. Morad, M. Rafatullah and S.-A. Ong, Degradation of cationic and anionic dyes in coagulation–flocculation process using bi-functionalized silica hybrid with aluminum-ferric as auxiliary agent, *RSC Adv.*, 2015, **5**, 34206–34215.
3 G. La Scalia, R. Micale, L. Cannizzaro and F. P. Marra, A sustainable phenolic compound extraction system from

olive oil mill wastewater, *J. Cleaner Prod.*, 2017, **142**, 3782–3788.
4 H. Sepehrmansourie, H. Alamgholiloo, N. N. Pesyan and M. A. Zolfigol, A MOF-on-MOF strategy to construct double *Z*-scheme heterojunction for high-performance photocatalytic degradation, *Appl. Catal., B*, 2023, **321**, 122082.
5 Q. Li, Z. Chen, H. Wang, H. Yang, T. Wen, S. Wang, B. Hu and X. Wang, Removal of organic compounds by nanoscale zero-valent iron and its composites, *Sci. Total Environ.*, 2021, **792**, 148546.
6 Z. Xiong, H. Zhang, W. Zhang, B. Lai and G. Yao, Removal of nitrophenols and their derivatives by chemical redox: A review, *Chem. Eng. J.*, 2019, **359**, 13–31.
7 H. Liu, Y.-N. Qin, H.-Y. Li, L.-X. Gai, Q. An, S. Zhai, Z. Xiao and L. Cui, Promotional effect of embedded Ni NPs in alginate-based carbon toward Pd NPs efficiency for high-concentration p-nitrophenol reduction, *Int. J. Biol. Macromol.*, 2021, **173**, 160–167.
8 C. Gao, Q. An, Z. Xiao, S. Zhai, B. Zhai and Z. Shi, Alginate and polyethyleneimine dually mediated synthesis of nanosilver-containing composites for efficient p-nitrophenol reduction, *Carbohydr. Polym.*, 2018, **181**, 744–751.
9 Z.-Z. Wang, S.-R. Zhai, B. Zhai, Q.-D. An and S.-W. Li, In situ reduction and stabilization of Ag NPs onto magnetic composites for rapid hydrogenation catalysis, *J. Sol-Gel Sci. Technol.*, 2015, **75**, 680–692.
10 Z.-Z. Wang, S.-R. Zhai, B. Zhai and Q.-D. An, One-step green synthesis of multifunctional Fe_3O_4/Cu nanocomposites toward efficient reduction of organic dyes, *Eur. J. Inorg. Chem.*, 2015, 1692–1699.
11 K. Yasar, A. Recepoglu, Y. Goren, Y. Orooji, V. Vatanpour, N. Kudaibergenov and A. Khataee, Polyoxometalate-based hybrid composites in multi-functional wastewater treatment applications, *J. Water Proc. Eng.*, 2023, **53**, 103863.
12 Y. Zhang, D.-H. Yang, S. Qiao and B.-H. Han, Synergistic catalysis of ionic liquid-decorated covalent organic frameworks with polyoxometalates for CO_2 cycloaddition reaction under mild conditions, *Langmuir*, 2021, **37**, 10330–10339.
13 N. Aramesh, B. Yadollahi and V. Mirkhani, Fe(III) substituted Wells–Dawson type polyoxometalate: An efficient catalyst for ring opening of epoxides with aromatic amines, *Inorg. Chem. Commun.*, 2013, **28**, 37–40.
14 Y. Ma, Y. Jiang, X. Wei, Q. Peng, S. Dai and Z. Hou, Hydrocarboxylation of olefins catalyzed by polyoxometalate-anchored palladium single-atom catalysts, *ACS Sustainable Chem. Eng.*, 2022, **10**, 15389–15401.
15 J. Lan, Y. Wang, B. Huang, Z. Xiao and P. Wu, Application of polyoxometalates in photocatalytic degradation of organic pollutants, *Nanoscale Adv.*, 2021, **3**, 4646–4658.
16 Y. Wu and L. Bi, Research progress on catalytic water splitting based on polyoxometalate/semiconductor composites, *Catalysis*, 2021, **11**, 524.
17 Y. Zou, H. Li, X. Zhao, J. Song, Y. Wang, P. Ma, J. Niu and J. Wang, Ru(III)-based polyoxometalate tetramers as highly efficient heterogeneous catalysts for alcohol oxidation reactions at room temperature, *Dalton Trans.*, 2021, **50**, 12664–12673.
18 N. Aramesh and B. Yadollahi, Polyoxometalate-based graphitic carbon nitride for reduction of toxic nitro aromatic compounds in water, *Mater. Chem. Phys.*, 2023, **296**, 127308.
19 K. Xia, K. Yamaguchi and K. Suzuki, Recent advances in hybrid materials of metal nanoparticles and polyoxometalates, *Angew. Chem., Int. Ed.*, 2023, **62**, e202214506.
20 S. Zhang, N. Liu, H. Wang, Q. Lu, W. Shi and X. Wang, Sub-nanometer nanobelts based on titanium dioxide/zirconium dioxide-polyoxometalate heterostructures, *Adv. Mater.*, 2021, **33**, 2100576.
21 P. Wang, L. Jiang, X. Zou, H. Tan, P. Zhang, J. Li, B. Liu and G. Zhu, Confining polyoxometalate clusters into porous aromatic framework materials for catalytic desulfurization of dibenzothiophene, *ACS Appl. Mater. Interfaces*, 2020, **12**, 25910–25919.
22 J. M. Park, C. M. Kim and S. H. Jhung, Melamine/polyaniline-derived carbons with record-high adsorption capacities for effective removal of phenolic compounds from water, *Chem. Eng. J.*, 2021, **420**, 127627.
23 Z. Akbari, S. J. Hoseini, M. Bahrami, R. Hashemi Fath, M. Montazerozohori and S. M. Nabavizadeh, Palladium/melamine-based porous network thin film at oil/water interface as effective catalyst for reduction of *p*-nitrophenol to *p*-aminophenol and dye degradation, *Microporous Mesoporous Mater.*, 2022, **330**, 111612.
24 S. A. Bhat, F. Zafar, A. H. Mondal, A. U. Mirza, Q. M. Rizwanul Haq and N. Nishat, Efficient removal of Congo red dye from aqueous solution by adsorbent films of polyvinyl alcohol/melamine-formaldehyde composite and bactericidal effects, *J. Cleaner Prod.*, 2020, **255**, 120062.
25 G. Wang, K. Lv, T. Chen, Z. Chen and J. Hu, Immobilizing of palladium on melamine functionalized magnetic chitosan beads: A versatile catalyst for *p*-nitrophenol reduction and Suzuki reaction in aqueous medium, *Int. J. Biol. Macromol.*, 2021, **184**, 358–368.
26 J. Jiao, H. Sun, C. Si, J. Xu, T. Zhang and Q. Han, Photocatalytic multielectron reduction of nitroarenes to anilines by utilizing an electron-storable polyoxometalate-based metal–organic framework, *ACS Appl. Mater. Interfaces*, 2022, **14**, 16386–16393.
27 S. D. Kurbah, Development of sustainable and efficient nanocatalyst based on polyoxometalate/nickel oxide nanocomposite: A simple and recyclable catalyst for reduction of nitroaromatic compounds, *J. Chin. Chem. Soc.*, 2021, **68**, 1487–1495.
28 A. D. Stergiou, D. H. Broadhurst and M. D. Symes, Highly selective electrocatalytic reduction of substituted nitrobenzenes to their aniline derivatives using a polyoxometalate redox mediator, *ACS Org. Inorg. Au*, 2023, **3**, 51–58.
29 R. Haddad and A. Roostaie, Nano-polyoxotungstate $[Cu_{20}P_8W_{48}]$ immobilized on magnetic nanoparticles as an excellent heterogeneous catalyst nanoreactors for green reduction of nitrophenol compounds, *J. Spectrosc.*, 2022, 7019037.

30 A. D. Niatouri and B. Yadollahi, A novel POM/LDH/GO nanocomposite as highly efficient heterogeneous catalyst in green epoxidation of alkenes with hydrogen peroxide, *Catal. Commun.*, 2023, **185**, 106808.
31 M. Aghayi, B. Yadollahi and M. R. Farsani, Zinc substituted Keggin-type polyoxometalate on Dowex: A green heterogeneous catalyst for oxidation of alcohols in water, *J. Iran. Chem. Soc.*, 2020, **17**, 2895–2900.
32 N. E. Mircescu, M. Oltean, V. Chiș and N. Leopold, FTIR, FT-Raman, SERS and DFT study on melamine, *Vib. Spectrosc.*, 2012, **62**, 165–171.
33 S. Jawaid, F. N. Talpur, H. I. Afridi, S. M. Nizamani, A. A. Khaskheli and S. Naz, Quick determination of melamine in infant powder and liquid milk by Fourier transform infrared spectroscopy, *Anal. Methods*, 2014, **6**, 5269–5273.
34 C. Wang, H. Fan, X. Ren, J. Fang, J. Ma and N. Zhao, Porous graphitic carbon nitride nanosheets by pre-polymerization for enhanced photocatalysis, *Mater. Charact.*, 2018, **139**, 89–99.
35 P. Shringarpure, B. K. Tripuramallu, K. Patel and A. Patel, Synthesis, structural, and spectral characterization of Keggin-type mono cobalt(II)-substituted phosphotungstate, *J. Coord. Chem.*, 2011, **64**, 4016–4028.
36 N. Zhang, P. Chen, W. Chen, H. Zhang and Y. Wang, Supramolecular self-assembly of nickel(II)-substituted α-Keggin-type polyoxometalate and polyaniline coated Fe_2O_3 hollow nanospindle for microwave absorption application, *Prog. Nat. Sci.: Mater. Int.*, 2021, **31**, 387–397.
37 S. Lin, X. Zhang and M. Luo, A novel inorganic-organic hybrid compound constructed from copper(II)-monosubstituted polyoxometalates and poly(amidoamine), *J. Solid State Electrochem.*, 2009, **13**, 1585–1589.
38 N. Sahiner, S. Demirci and K. Sel, Covalent organic framework based on melamine and dibromoalkanes for versatile use, *J. Porous Mater.*, 2016, **23**, 1025–1035.
39 J.-S. Shen, Q.-G. Cai, Y.-B. Jiang and H.-W. Zhang, Anion-triggered melamine based self-assembly and hydrogel, *Chem. Commun.*, 2010, **46**, 6786–6788.
40 H. Chi, B. Liu, G. Guan, Z. Zhang and M.-Y. Han, A simple, reliable and sensitive colorimetric visualization of melamine in milk by unmodified gold nanoparticles, *Analyst*, 2010, **135**, 1070–1075.
41 M. X. Tan, Y. N. Sum, J. Y. Ying and Y. Zhang, Mesoporous poly-melamine-formaldehyde polymer as a solid sorbent for toxic metal removal, *Energy Environ. Sci.*, 2013, **6**, 3254–3259.
42 Y. Hua, M. Liu, S. Li, F. Liu, Y. Cai, H. Liu, Y. Wan, X. Lv and H. Wang, An electroanalysis strategy for glutathione in cells based on the displacement reaction route using melamine-copper nanocomposites synthesized by the controlled supermolecular self-assembly, *Biosens. Bioelectron.*, 2019, **124**, 89–95.
43 A. B. Wiles, D. Bozzuto, C. L. Cahill and R. D. Pike, Copper(I) and (II) complexes of melamine, *Polyhedron*, 2006, **25**, 776–782.
44 F. Chen, X. Yan, X. Hu, R. Feng, T. Li, X. Li and G. Zhao, Enhanced catalytic reduction of p-nitrophenol and azo dyes on copper hexacyanoferrate nanospheres decorated copper foams, *J. Environ. Manage.*, 2022, **314**, 115075.
45 N. T. Al-Thakafy, M. S. Al-Enizzi and M. Y. Saleh, Synthesis of new organic reagent by Vilsmeier-Haack reaction and estimation of pharmaceutical compounds (Mesalazine) containing aromatic amine groups, *Egypt. J. Chem.*, 2022, **65**, 685–697.
46 S. J. Hoseini, M. Bahrami, N. Sadri, N. Aramesh, Z. Samadi Fard, H. Rafatbakhsh Iran, B. Habib Agahi, M. Maddahfar, M. Dehghani, A. Zarei Baba Arabi, N. Heidari, S. F. Hashemi Fard and Z. Moradi, Multi-metal nanomaterials obtained from oil/water interface as effective catalysts in reduction of 4-nitrophenol, *J. Colloid Interface Sci.*, 2018, **513**, 602–616.
47 M. Aazza, H. Ahlafi, H. Moussout, C. Mounir, A. Fadel and A. Addad, Catalytic reduction of nitro-phenolic compounds over Ag, Ni and Co nanoparticles catalysts supported on γ-Al_2O_3, *J. Environ. Chem. Eng.*, 2020, **8**, 103707.
48 S. B. Khan, E. M. Bakhsh, K. Akhtar, T. Kamal, Y. Shen and A. M. Asiri, Copper oxide-antimony oxide entrapped alginate hydrogel as efficient catalyst for selective reduction of 2-nitrophenol, *Polymers*, 2022, **14**, 458.
49 N. M. Dat, P. N. B. Long, D. C. U. Nhi, N. N. Minh, L. M. Duy, L. N. Quan, H. M. Nam, M. T. Phong and N. H. Hieu, Synthesis of silver/reduced graphene oxide for antibacterial activity and catalytic reduction of organic dyes, *Synth. Met.*, 2020, **260**, 116260.
50 S. M. Albukhari, M. Ismail, K. Akhtar and E. Y. Danish, Catalytic reduction of nitrophenols and dyes using silver nanoparticles@cellulose polymer paper for the resolution of waste water treatment challenges, *Colloids Surf., A*, 2019, **577**, 548–561.
51 A. Z. Asadabadi, S. J. Hoseini, M. Bahrami and S. M. Nabavizadeh, Catalytic applications of β-cyclodextrin/palladium nanoparticle thin film obtained from oil/water interface in the reduction of toxic nitrophenol compounds and the degradation of azo dyes, *New J. Chem.*, 2019, **43**, 6513–6522.
52 A. A. Kassem, H. N. Abdelhamid, D. M. Fouad and S. A. Ibrahim, Hydrogenation reduction of dyes using metal–organic framework-derived CuO@C, *Microporous Mesoporous Mater.*, 2020, **305**, 110340.
53 S. Jamil, Z. Ahmad, M. Ali, S. R. Khan, S. Ali, M. A. Hammami, M. Haroon, T. A. Saleh and M. R. S. A. Janjua, Synthesis and characterization of polyaniline/nickel oxide composites for fuel additive and dyes reduction, *Chem. Phys. Lett.*, 2021, **776**, 138713.
54 H. Yin, Y. Kuwahara, K. Mori, M. Che and H. Yamashita, Plasmonic Ru/hydrogen molybdenum bronze with tunable oxygen vacancies for light-driven reduction of *p*-nitrophenol, *J. Mater. Chem. A*, 2019, **7**, 3783–3789.
55 W. A. Shaha, L. Noureen, M. A. Nadeem and P. Kögerler, Encapsulation of Keggin-type manganese-polyoxomolybdates in MIL-100 (Fe) for efficient reduction of p-nitrophenol, *J. Solid State Chem.*, 2018, **268**, 75–82.
56 T. Li, Z. Zhang, L. Liu, M. Gao and Z. Han, A stable metal–organic framework nanofibrous membrane as photocatalyst for simultaneous removal of methyl orange and formaldehyde from aqueous solution, *Microporous Mesoporous Mater.*, 2021, **617**, 126359.

57 K. Mubeen, A. Irshad, A. Safeen, U. Aziz, K. Safeen, T. Ghani, K. Khan, Z. Ali, I. Haq and A. Shah, Band structure tuning of ZnO/CuO composites for enhanced photocatalytic activity, *J. Saudi Chem. Soc.*, 2023, **27**, 101639.

58 A. Sanguino, C. Diaz-Uribe, F. Duran, W. Vallejo, L. Guzman, D. Ruiz, E. Puello, C. Quiñones, E. Schott and X. Zarate, Photocatalytic degradation of methylene blue under visible light using TiO_2 thin films impregnated with porphyrin and Anderson-type polyoxometalates (Cu and Zn), *Catalysts*, 2022, **12**, 1169.

59 S. Bharath, A. Lazer, Y.-L. Lin, P. Peter and J. Thavasikani, Novel morphological mono-metallic substituted polyoxometalate immobilized 3-(aminopropyl)-imidazole photocatalysts for visible-light driven degradation: Anti-bacterial activity, membrane bacterial activity applications, *Spectrochim. Acta, Part A*, 2023, **299**, 122868.

60 M. Ismail, M. I. Khan, S. B. Khan, M. A. Khan, K. Akhtar and A. M. Asiri, Green synthesis of plant supported Cu–Ag and Cu–Ni bimetallic nanoparticles in the reduction of nitrophenols and organic dyes for water treatment, *J. Mol. Liq.*, 2018, **260**, 78–91.